GEOPHYSICS, VOL. 81, NO. 6 (NOVEMBER-DECEMBER 2016); P. S469–S475, 5 FIGS.
10.1190/GEO2016-0113.1

Attenuating multiple-related imaging artifacts using combined imaging conditions

Carlos Alberto da Costa Filho[1] and Andrew Curtis[1]

ABSTRACT

The objective of prestack depth migration is to position reflectors at their correct subsurface locations. However, migration methods often also generate artifacts along with physical reflectors, which hamper interpretation. These spurious reflectors often appear at different spatial locations in the image depending on which migration method is used. Therefore, we have devised a postimaging filter that combines two imaging conditions to preserve their similarities and to attenuate their differences. The imaging filter is based on combining the two constituent images and their envelopes that were obtained from the complex vertical traces of the images. We have used the method to combine two images resulting from different migration schemes, which produce dissimilar artifacts: a conventional migration method (equivalent to reverse time migration) and a deconvolution-based imaging method. We show how this combination may be exploited to attenuate migration artifacts in a final image. A synthetic model containing a syncline and stochastically generated small-scale heterogeneities in the velocity and density distributions was used for the numerical example. We compared the images in detail at two locations where spurious events arose and also at a true reflector. We found that the combined imaging condition has significantly fewer artifacts than either constituent image individually.

INTRODUCTION

Seismic imaging converts seismic data into a map of the subsurface that should only contain true structures that reflect seismic energy. However, imaging methods also map spurious reflectors — features that do not correspond to the true subsurface structure. These may be caused by unattenuated multiples, imaging condition artifacts, limited aperture, aliasing, random noise, and many other factors.

Of particular importance are artifacts caused by unattenuated multiples because these frequently hamper interpretation. Conventional imaging approaches such as reverse time migration (RTM) (Baysal et al., 1983) and Kirchhoff migration (Schneider, 1978) are based on the single-scattering approximation, which presupposes that the data are free of multiples. Free-surface multiples (those which have a downward reflection on the sea or land surface) can be attenuated using a variety of methods, a review of which can be found in Verschuur (2006). Unlike free-surface multiples, whose downward reflections occur at the known earth's surface, internal multiples have a downward reflections at a priori unknown subsurface interfaces making their detection, prediction, and attenuation much more difficult. We present a new method to mitigate the effects of internal multiples on the seismic image, although we note that the same method can also be used for free-surface multiples and potentially other forms of noise.

Internal multiples are most commonly attenuated in the data prior to carrying out imaging. For example, using Rayleigh's reciprocity theorem, Fokkema et al. (1994) derive equations to remove multiples from a known subsurface interface. Weglein et al. (1997) use a Lippmann-Schwinger scattering series to remove internal multiples without knowledge of subsurface reflectors. Jakubowicz (1998) shows how combinations of primaries could be used to remove internal multiples based on the theory of Berkhout and Verschuur (1997). Using a similar description of wave propagation, the common-focus-point method predicts and subsequently removes internal multiples (Berkhout and Verschuur, 2005). Imaging condition approaches to remove the effects of such multiples include using the Poynting vector (Richardson and Malcolm, 2014), deconvolution (Valenciano and Biondi, 2003), and local slopes (Sava, 2007). Postimaging approaches include filtering common-image gathers (Biondi and Shan, 2002) or filtering the final image (Youn and Zhou, 2001; Guitton et al., 2007). Multiple prediction methods may also be used to identify multiples in the migrated section to aid interpretation. In this case, multiples may be estimated in the data domain

Manuscript received by the Editor 3 March 2016; revised manuscript received 31 May 2016; published online 29 September 2016.
[1]University of Edinburgh, Grant Institute, Edinburgh, UK. E-mail: c.costa@ed.ac.uk; andrew.curtis@ed.ac.uk.

and then migrated, or directly estimated in the migration domain (Wang et al., 2009). This should reduce the likelihood of artifacts being interpreted as real reflectors.

Another approach is to use multiply scattered waves for imaging. Much work has been devoted to imaging using surface-related multiples (Reiter et al., 1991; Berkhout and Verschuur, 1994, 2006; Guitton, 2002; Shan, 2003; Muijs et al., 2007), but considerably less has been achieved using internal multiples. The first such method was developed by Youn and Zhou (2001), and it required a detailed velocity model a priori. Data-driven methods such as interferometric imaging have become popular especially for vertical seismic profile data (Schuster et al., 2004; Vasconcelos et al., 2008). Malcolm et al. (2009) propose an imaging method for internal multiples based on inverse scattering, Fleury (2013) develops an RTM scheme that includes internal multiples, and Zuberi and Alkhalifah (2014) use doubly scattered wavefields to better image steep dips. Full-wavefield migration (Berkhout, 2012) migrates internal multiples (alongside primaries and surface multiples) given an excellent velocity model, which may be provided by full-wavefield inversion at high computational cost.

Despite this array of existing methods, the effects of internal multiples still affect images significantly because no current method works well and is robust in all situations. Recently, a new inverse-scattering theory based on the Marchenko equation has been developed for acoustic (Broggini and Snieder, 2012; Wapenaar et al., 2013) and elastodynamic (da Costa Filho et al., 2014; Wapenaar, 2014) wavefields. This constructs virtual responses (which would be recorded) at any location interior to the medium from surface sources, using only surface reflection data and a smooth estimate of the velocity macromodel. Marchenko inverse scattering may also be used to predict and remove internal multiples in acoustic (Meles et al., 2015) and elastic (da Costa Filho et al., forthcoming) data. Imaging methods that use wavefields from the Marchenko methods have been referred to as data-driven wavefield imaging (Broggini et al., 2014), autofocus imaging (Behura et al., 2014; da Costa Filho et al., 2015), and Marchenko imaging (Wapenaar et al., 2014).

Conventional migration methods combine a synthetically modeled source wavefield with the back-propagated recorded seismic wavefield to perform imaging, in which neither wavefield accounts for multiple scattering from the unknown earth structure (Claerbout, 1985). Marchenko methods construct subsurface down- and upgoing fields that include such multiple scattering. Even though these fields may be used at high computational expense to obtain artifact-free images through multidimensional deconvolution (MDD), single-channel deconvolution (SCD) may be used to obtain images more cheaply. Although this and conventional migration methods are able to image the true reflectors, they also create spurious reflectors, often at different locations in the images.

We introduce a general method to combine any two imaging conditions that retains the phase of waves associated with true reflectors. We choose to combine conventional crosscorrelational RTM and SCD of Marchenko fields to illustrate how the method can be used to retain true reflectors and attenuate artifacts. Conventional imaging is chosen because of its ubiquity, and SCD Marchenko imaging because it approximates MDD of Marchenko fields, but with far lower computational cost. A synthetic example shows that the combined method improves on RTM and SCD Marchenko imaging, strongly attenuating their multiple-related artifacts.

The idea of combining images and data sets is well-known in seismic processing and migration. Common-midpoint stacking (Yilmaz, 2001) has been used to attenuate instrument noise and can be regarded as a summation of all substacks. Summing multiple sources in shot-profile migration attenuates migration artifacts (Berkhout, 1985) and can be regarded as summing partial images over each source. Using multiple azimuths often improves illumination (in multi- or wide-azimuth towed-streamer surveys) (Regone, 2007), which again might be regarded as summing over images from each azimuth.

These methods are effective because they exploit the intrinsic linearity of the wave equation and assumed linearity of other processing steps, whereby summation of different data is, in principle (in the absence of variable preprocessing), equivalent to summing over the resulting images from those different data. Our method is different: It is applicable to images that bear no relationship to each other apart from imaging the same structures; it does not assume linearity of either the imaging method or the preprocessing steps; and it is also not a simple sum because this was found to produce significantly poorer results. In what follows, we present the method, apply it to a synthetic example, and discuss its application to a wide range of imaging methods.

METHODS

All conventional wave-equation-based imaging methods, such as RTM and Kirchhoff prestack migration, image the true reflectors by combining (e.g., by crosscorrelating or deconvolving) incoming and outgoing wavefields at each point of the image. The incoming field is commonly obtained by forward propagating a synthetic source wavelet in a reference model, which is usually smooth but may contain specific discontinuities (e.g., the seabed or the boundaries of a salt body). In RTM, this is usually done by finite-difference modeling and can also be achieved through ray tracing as is common in Kirchhoff migration. To estimate the outgoing field, the recorded reflection data are back-propagated through the same reference medium into the subsurface. These wavefields are then combined with an imaging condition such as crosscorrelation or deconvolution to create the final image. In smooth media, the incoming wavefield is downgoing and the outgoing wavefield is often upgoing and to remain consistent with the Marchenko literature this is the terminology used hereafter.

Let $G^{\pm}(\mathbf{x}_I, \mathbf{x}_S, t)$ denote the downgoing (+) and upgoing (−) wavefields measured at subsurface image point $\mathbf{x}_I$ from a surface source $\mathbf{x}_S$. The downgoing field in conventional methods is approximated as

$$G^{+}(\mathbf{x}_I, \mathbf{x}_S, t) \approx G^{0}(\mathbf{x}_I, \mathbf{x}_S, t), \tag{1}$$

where $G^{0}(\mathbf{x}_I, \mathbf{x}_S, t)$ is Green's function response of a known reference medium. The back-propagated wavefield is usually approximated as

$$G^{-}_{\mathrm{RTM}}(\mathbf{x}_I, \mathbf{x}_S, t) = \int_{\partial \mathbb{D}_S} R(\mathbf{x}_S, \mathbf{x}_R, t) * G^{0}(\mathbf{x}_I, \mathbf{x}_R, -t) \mathrm{d}^2\mathbf{x}_R, \tag{2}$$

where $R(\mathbf{x}_S, \mathbf{x}_R, t)$ is the measured reflection response with ghosts and surface-related multiples removed and with the source wavelet deconvolved, $*$ denotes temporal convolution, $\partial \mathbb{D}_S$ represents the seismic acquisition surface datum, and the exact expression for which equation 2 is an approximation is given by Halliday and Curtis (2010) for acoustic media and Ravasi and Curtis (2013)

for elastic media. The removal of free-surface multiples from R may be unnecessary if the method of Singh et al. (2015) is used, although that is not attempted here. The quantity in equation 2 is used to approximate the true upgoing field $G^-(\mathbf{x}_I, \mathbf{x}_S, t)$. We define a reference imaging condition for conventional migration as the zero time lag crosscorrelation between the approximate up- and downgoing fields, summed over source positions

$$I_{\mathrm{C}}(\mathbf{x}_I) = \sum_{\mathbf{x}_S} G^0(\mathbf{x}_I, \mathbf{x}_S, -t) * G^-_{\mathrm{RTM}}(\mathbf{x}_I, \mathbf{x}_S, t)|_{t=0}, \quad (3)$$

or in the frequency domain

$$I_{\mathrm{C}}(\mathbf{x}_I) = \sum_{\mathbf{x}_S} \int_{-\infty}^{\infty} G^0(\mathbf{x}_I, \mathbf{x}_S, \omega)^* G^-_{\mathrm{RTM}}(\mathbf{x}_I, \mathbf{x}_S, \omega) \mathrm{d}\omega, \quad (4)$$

where superscript $*$ represents complex conjugation.

Marchenko inverse-scattering theory uses R and the direct wave in G^0 to construct virtual seismic data gathers at subsurface virtual receivers from surface sources that include all internal multiples. The algorithm we use to obtain these wavefields is given in Wapenaar et al. (2013). This improves the estimate of the down- and upgoing wavefields at each image point. Here, we combine these wavefields through a single-channel regularized deconvolutional imaging condition in the frequency domain

$$I_D(\mathbf{x}_I) = \sum_{\mathbf{x}_S} \int_{-\infty}^{\infty} \frac{G^+_{\mathrm{M}}(\mathbf{x}_I, \mathbf{x}_S, \omega)^* G^-_{\mathrm{M}}(\mathbf{x}_I, \mathbf{x}_S, \omega)}{|G^+_{\mathrm{M}}(\mathbf{x}_I, \mathbf{x}_S, \omega)|^2 + \varepsilon \max\limits_{\mathbf{x}_S, \omega} |G^+_{\mathrm{M}}(\mathbf{x}_I, \mathbf{x}_S, \omega)|^2} \mathrm{d}\omega, \quad (5)$$

where G^+_{M} and G^-_{M} are Marchenko estimates of the down- and upgoing fields and ε is a regularization factor that we took to be 10^{-2}. Pioneered by Behura et al. (2014) as deconvolutional "autofocus imaging," and referred to as "data-driven wavefield imaging" by Broggini et al. (2014), we refer to it more specifically as SCD of Marchenko fields to differentiate from the related but far more computationally demanding MDD-based imaging of Marchenko fields (Wapenaar et al., 2014).

Even though RTM and SCD Marchenko methods image the true reflectors correctly, they both contain spurious reflectors generated by crosstalk between unrelated events. This may be expressed as

$$I_{\mathrm{C}}(\mathbf{x}_I) = I_{\mathrm{T}}(\mathbf{x}_I) + \acute{I}_{\mathrm{C}}(\mathbf{x}_I), \quad (6)$$

$$I_{\mathrm{D}}(\mathbf{x}_I) = I_{\mathrm{T}}(\mathbf{x}_I) + \acute{I}_{\mathrm{D}}(\mathbf{x}_I), \quad (7)$$

where I_{T} is the "true" image devoid of such artifacts and $\acute{I}_{\mathrm{C}}$ and $\acute{I}_{\mathrm{D}}$ are the crosstalk terms that cause the artifacts. Importantly, this assumes that I_{C} and I_{D} produce images with equal phase for true reflectors.

Crosstalk terms $\acute{I}_{\mathrm{C}}$ and $\acute{I}_{\mathrm{D}}$ are inherently different from each other because they arise from the combination of different wavefields: $\acute{I}_{\mathrm{C}}$ is caused by the crosscorrelation of the direct downgoing wave with the internal multiples back-propagated (erroneously) through a mainly smooth reference model. These events do not appear in $\acute{I}_{\mathrm{D}}$ as internal multiples in the reflection data are not back-propagated. Rather, G^-_M in equation 5 is the correctly redatumed response at a virtual receiver in the subsurface from a surface source. In these virtual gathers, multiples in the data are mapped to arrival times that correspond to physical higher order reflections from a surface virtual source. Thus, internal multiples in G^-_M arrive after the direct wave and never crosscorrelate constructively with the direct wave in I_{D}. However, other kinds of artifacts are present in I_{D}: internal multiples in G^+_{M}, that is, internal multiples that arrive downgoing at the virtual receiver, may interact with unrelated events in G^-_{M}, that is, events that arrive upgoing at the virtual receiver, creating artifacts $\acute{\mathrm{I}}_{\mathrm{D}}$. Because of the different nature of artifacts in $\acute{I}_{\mathrm{C}}$ and $\acute{I}_{\mathrm{D}}$, they generally appear at different image points (for a more in-depth explanation of these artifacts, see da Costa Filho et al., 2015).

It should therefore be possible to combine I_{C} and I_{D} so as to preserve the true image I_{T} while attenuating the artifacts $\acute{I}_{\mathrm{C}}$ and $\acute{I}_{\mathrm{D}}$. A simple multiplication of the two images destroys phase information of the true reflectors. Instead, we calculate the (real, nonnegative) amplitude envelopes of each image in the vertical direction, multiply each by the other image point-by-point, add the two resulting images, and normalize the result by the sum of the envelopes.

The Hilbert transform is used to calculate envelopes of a vertical line within an image $I(z)$. It phase shifts the positive (here, spatial) frequencies of a real image $I(z)$ by $-90°$ and the negative frequencies by 90° and can be defined as

$$H[I] = \mathcal{F}^{-1}[-i\,\mathrm{sgn}(k_z)\mathcal{F}[I]], \quad (8)$$

where $\mathcal{F}$ denotes the Fourier transform, sgn denotes the sign function, and k_z is the vertical spatial frequency. The (real, positive) amplitude envelope of the signal is defined as

$$E[I](\mathbf{x}) = \sqrt{I(z)^2 + H[I](z)^2}. \quad (9)$$

Figure 1 shows an example of a real-valued signal $I(z)$, its Hilbert transform $H[I](z)$, and its envelope $E[I](z)$ showing clearly that the envelope is real and nonnegative, and it can be thought of as an upper bound on the seismic oscillations.

Therefore, we define the combined imaging condition

$$I_{\mathrm{H}}(\mathbf{x}_I) = \frac{E[I_{\mathrm{C}}](\mathbf{x}_I) I_{\mathrm{D}}(\mathbf{x}_I) + E[I_{\mathrm{D}}](\mathbf{x}_I) I_{\mathrm{C}}(\mathbf{x}_I)}{E[I_{\mathrm{C}}](\mathbf{x}_I) + E[I_{\mathrm{D}}](\mathbf{x}_I)}, \quad (10)$$

where the envelope E is applied to each vertical trace throughout the image at each fixed horizontal position. The effect of the numerator

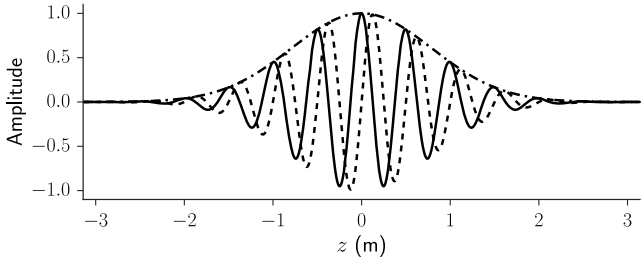

Figure 1. The solid line depicts an example real-valued signal $I(z) = e^{-0.8z^2}\cos(4\pi z)$. The dashed line shows its Hilbert transform $H[I](z) = e^{-0.8z^2}\sin(4\pi z)$. The dotted-dashed line shows its envelope $E[I](z) = e^{-0.8z^2}$.

in equation 10 is to detect and modulate the amplitudes in the different images, ensuring that events present in both are amplified, and those only present in one are attenuated. The denominator serves to normalize the amplitudes that are squared in the numerator.

In the simplest case of nonintersecting supports of I_T, $\acute{I}_C$, and $\acute{I}_D$ (i.e., they are never nonzero at the same image point), we may simplify the expression in equation 10:

$$\begin{aligned} I_H &= \frac{E[I_T+\acute{I}_C](I_T+\acute{I}_D)+E[I_T+\acute{I}_D](I_T+\acute{I}_C)}{E[I_T]+E[\acute{I}_C]+E[I_T]+E[\acute{I}_D]} \\ &= \frac{2E[I_T]I_T+E[I_T](\acute{I}_D+\acute{I}_C)+E[\acute{I}_C](I_T+\acute{I}_D)+E[\acute{I}_D](I_T+\acute{I}_C)}{2E[I_T]+E[\acute{I}_C]+E[\acute{I}_D]} \\ &= I_T, \end{aligned} \tag{11}$$

where we have suppressed notational dependence on $\mathbf{x}_I$. We thus show that in this case, the combined imaging condition retains the same relative amplitudes as the true image, whereas removing crosstalks $\acute{I}_C$ and $\acute{I}_D$. The denominator in equation 10 may become zero when $\mathbf{x}_I$ is reflection free. In this case, a regularization factor such as $\varepsilon \max_{\mathbf{x}_I}\{E[I_C](\mathbf{x}_I) + E[I_D](\mathbf{x}_I)\}$ may be added to the denominator, similarly to equation 5. However, in the presence of noise, this may not be required and, in fact, is not used in the following example.

Even though the present method combines only two constituent images, there are several ways in which to extend it to an arbitrary number of envelopes. However, we do not consider them further here and focus on combining two images.

NUMERICAL EXAMPLE

Our synthetic model consists of reflectors and stochastically distributed density and velocity variations — Figure 2a shows its bulk modulus. The reflection data without surface-related multiples or ghosts were obtained using 2D time-domain finite-difference modeling with absorbing boundary conditions on all sides, followed by removal of the direct wave and source wavelet deconvolution. The Marchenko method requires a wide-aperture, dense sampling of sources and receivers, which must be colocated. We used fixed receivers placed between 0 and 2.5 km separated by 12 m; a shot was placed at the position of each receiver in turn. Behura et al. (2014) discuss how to obtain fixed-spread gathers from conventional marine acquisition, and for other types of acquisition suitably redatumed data may be constructed by preprocessing (e.g., for ocean bottom data, see Ravasi et al., 2015, 2016).

Conventional and SCD Marchenko imaging also require estimates of the direct wave from each source to subsurface imaging locations. We used an eikonal solver (Fomel, 1997) on a smoothed version of the medium to calculate the traveltimes of direct waves from surface sources to each image point. Direct waveforms were estimated by placing a wavelet with central frequency of 20 Hz at the appropriate traveltimes and scaling each trace by $1/\sqrt{t}$. We imaged the model using the conventional and deconvolutional Marchenko imaging schemes, as shown in Figure 2b and 2c, respectively. Equation 10 was then used to generate the combined image I_H in Figure 2d.

DISCUSSION

Images in Figure 2b and 2c show the recovery of the three true reflectors caused by the discontinuities in bulk modulus shown in Figure 2a; the stochastic heterogeneities disturb the propagating waves but do not create strong diffractions and hence are not individually imaged. Both of these images are contaminated by spuri-

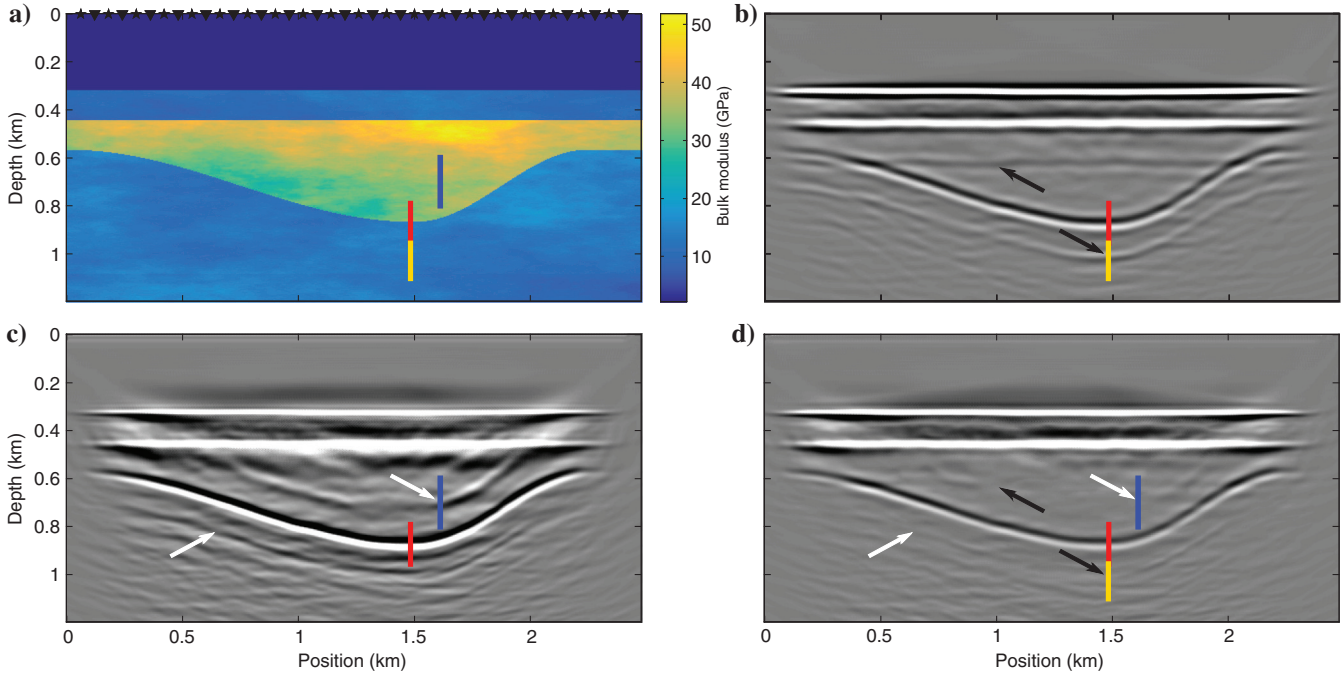

Figure 2. (a) Synthetic model with four layers and stochastically distributed heterogeneities. Sources and receivers are colocated along the top boundary. (b) Conventional RTM image, (c) deconvolutional Marchenko image, and (d) combined image. Arrows indicate spurious reflectors in panels (b and c), and are duplicated in panel (d). The colored vertical lines show locations of individual traces that are displayed in Figures 3 (yellow), 4 (blue), and 5 (red).

ous artifacts resulting from internal multiples as indicated by arrows. The conventional image is contaminated by back-propagated internal multiples, one of which appears under the lowest flat reflector, and another immediately below the true synclinal reflector. SCD Marchenko imaging also produces artifacts that, as expected, generally occur at different positions compared with the conventional image. For example, the artifact immediately above the synclinal interface indicated in Figure 2c results from the interaction between two unrelated up- and downgoing events that occur at the same time (for a kinematic explanation, see da Costa Filho et al., 2015).

The combined image annihilates almost all multiple-related artifacts despite the complex stochastic heterogeneities. Figure 2d outperforms conventional and deconvolutional Marchenko imaging showing only the true reflectors without any strong spurious artifacts. The only continuous events in Figure 2d are the true reflectors, whereas in Figure 2b and 2c spurious reflectors are also continuous. Thus, the combined imaging method should at least contribute to discriminate artifacts in the other two. The arrows in Figure 2 indicate the location of artifacts in the images, which have mostly been attenuated in the combined image. However, note that immediately to the left of the leftmost black arrow, there is a residual artifact as this is present in both of the constituent images.

Figures 3 and 4 show individual traces displaying artifacts and their comparison with the combined and true images. The true image used in these figures was obtained by computing the reflectivity from the acoustic impedance and convolving the result with a wavelet. Figure 3a shows a section of a single vertical trace centered around an artifact, which appears in the conventional image at $I_C(x = 1480\ \text{m}, z = 1008\ \text{m})$, whose location is indicated in the conventional image (Figure 2b) by the lower black arrow. Figure 3b shows the envelopes of these traces. Relative to local amplitudes, we see that the artifact in the conventional image (solid curve) is attenuated in the combined image. This is especially visible in the envelopes shown in Figure 3b where it can be seen that the main artifact is attenuated, whereas the traces in Figure 3a show that the artifact in the combined image is also less coherent than in the conventional image. A similar effect is seen with the SCD Marchenko image when compared with the combined image as shown in Figure 4. The artifact that appears in the SCD Marchenko image is shown by the upper white arrow in Figure 2c. The traces (Figure 4a) and their envelopes (Figure 4b) show that the artifact present in the SCD Marchenko image is severely attenuated in relation to local amplitudes in the combined image, approximating the true image more accurately.

Figure 5 shows a section of the normalized vertical traces taken at $x = 1480$ m centered around the true synclinal reflector at $z = 868$ m, depicted by the thin black lines. Figure 5a shows that the phase information that is the same in I_C and I_D is preserved in I_H. Figure 5b, on the other hand, shows how the vertical extension (resolution) of the combined image lies in between that of the conventional and SCD Marchenko images.

The marginal cost of creating the combination is negligible once SCD Marchenko imaging has been performed: In fact, the first iteration of Marchenko imaging requires the same downgoing

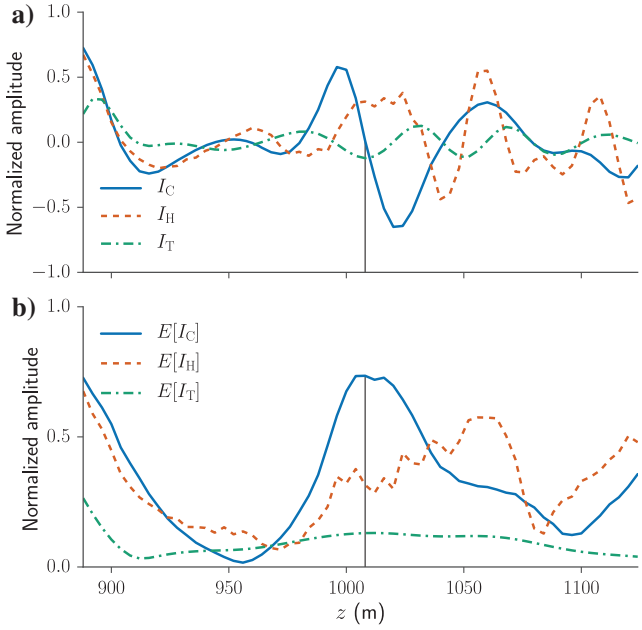

Figure 3. (a) Vertical sections at $x = 1480$ m of the conventional, combined, and true images, and (b) their envelopes. The location and extent of these traces are shown in Figure 2 by the yellow vertical lines. Traces related to the conventional method are shown as solid blue curves, those related to the combined images are shown as dashed orange curves, and those related to the true images are shown as dotted-dashed green lines. The envelope of the artifact in the conventional image peaks at $z = 1008$ m indicated by the thin black vertical lines and is attenuated in the combined image. Traces were taken from an AGC-equalized image to account for different amplitude scales.

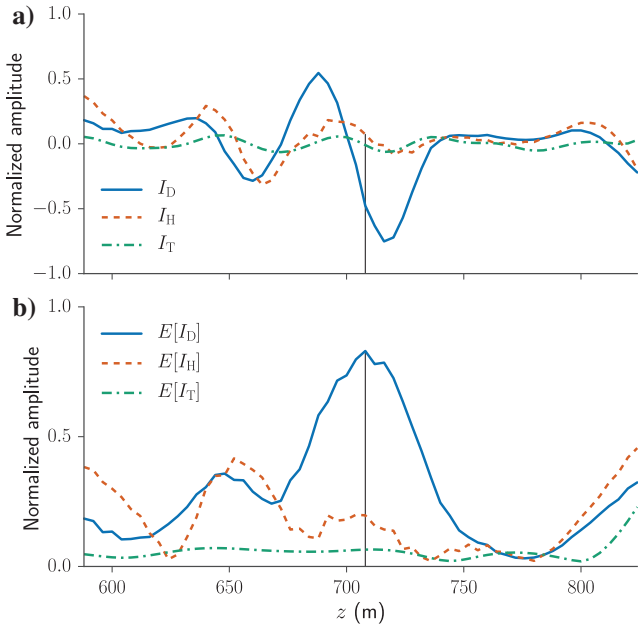

Figure 4. (a) Vertical sections at $x = 1600$ m of the SCD Marchenko, combined, and true images, and (b) their envelopes. The location and extent of these traces are shown in Figure 2 by the blue vertical lines. Traces related to the SCD Marchenko method are shown as solid blue curves, those related to the combined images are shown as dashed orange curves, and those related to the true images are shown as dotted-dashed green lines. The envelope of the artifact in the conventional image peaks at $z = 708$ m indicated by the thin black vertical lines and is attenuated in the combined image. Traces were taken from an AGC-equalized image to account for different amplitude scales.

wavefields and creates the upgoing wavefield (the integral in equation 2) required for conventional imaging. Hence, the only additional costs are to create the conventional image by correlating these wavefields and summing as in equation 3, and then calculating the combined image in equation 10. This makes the combined imaging condition extremely attractive in conjunction with SCD Marchenko imaging because it attenuates continuous spurious reflectors at almost no additional cost (of course, if only conventional imaging has been performed, performing Marchenko imaging requires considerable computational cost; Behura et al., 2014).

The combined imaging condition is not limited to the two imaging conditions used here: It may also be used to improve other imaging conditions, such as any of those proposed in Schleicher et al. (2008). The method may also be extended by using other envelope methods; for example, for steeply dipping reflectors, the vertical-trace Hilbert transform may be replaced by the 2D Hilbert transform (Stark, 1971). Even more generally, the method can be used as a way to preserve similarities between any pair of images while attenuating their differences.

Even though our example only contains internal multiple-related artifacts, other types of image artifacts may also be attenuated. For example, if RTM is performed in a model with interfaces, backscatter effects by the reflections of the back-propagated also cause artifacts; because these have different kinematic behavior to autofocus imaging, they would be attenuated. In general, the algorithm will perform better when there are fewer artifacts in either image, to reduce the chance of them intersecting.

Combining imaging conditions may not improve results if artifacts appear in the same locations with the same polarities in both images. It is also important to ensure that true reflectors are at the same positions in the constituent images: Using different wavelets or velocity models in the constituent imaging methods may vary the position or phase of reflections, causing them to be attenuated when combined. When differences in the images are only in wavelet shape or phase, applying spectral matching techniques to the migrated sections may be enough to provide suitable constituent images for the method. We conclude that if performed judiciously, this method can enhance the output of the constituent images, in this case obtained through conventional migration and SCD Marchenko imaging.

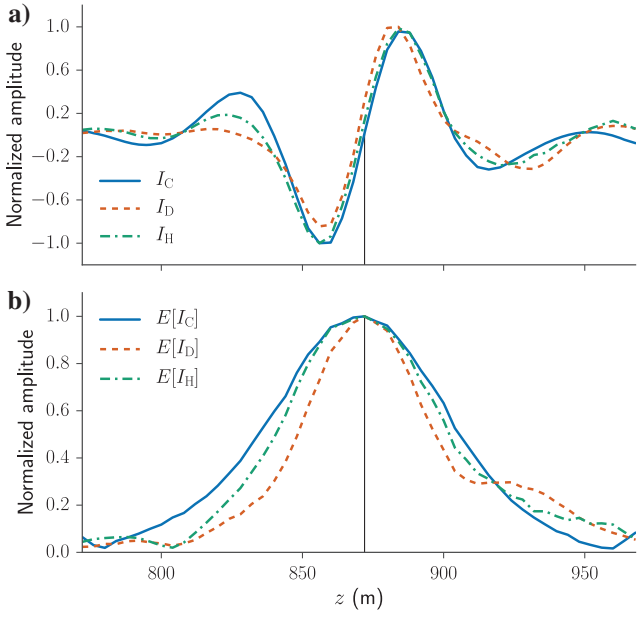

Figure 5. Resolution comparison between the different images. The location and extent of these traces are shown in Figure 2 by the red vertical lines. (a) A vertical section of the images at $x = 1480$ m centered around a true reflector at $z = 868$ m (thin black vertical line). The conventional image is depicted by the solid blue curve, the SCD Marchenko image by the dashed orange curve, and the combined image by the dotted-dashed green curve. (b) Envelope of traces in panel (a), with the same key. The reflector has the best vertical resolution using the SCD Marchenko image and the worse resolution using the conventional image. As expected, the combined image shows an intermediate resolution. Traces were normalized to their maximum inside the window for comparison.

CONCLUSION

We propose a general approach to combine pairs of images that retains their similarities and attenuates their differences. We apply the method to the problem of imaging with internal multiples by merging conventional imaging with SCD Marchenko imaging, using a postimaging combination of the two based on Hilbert transform envelopes. We demonstrate the method on an acoustic 2D model with stochastic velocity and density variations. Our results show that our combined image attenuates artifacts that result from internal multiples.

ACKNOWLEDGMENTS

We thank the Edinburgh Interferometry Project sponsors (ConocoPhillips, Schlumberger Gould Research, Statoil, and Total) for supporting this research. C. A. da Costa Filho would like to thank CAPES for funding. The authors thank associate editor I. Moore, K. Wapenaar, two anonymous reviewers and J. van der Neut for constructive suggestions.

REFERENCES

Baysal, E., D. D. Kosloff, and J. W. C. Sherwood, 1983, Reverse time migration: Geophysics, **48**, 1514–1524, doi: 10.1190/1.1441434.
Behura, J., K. Wapenaar, and R. Snieder, 2014, Autofocus imaging: Image reconstruction based on inverse scattering theory: Geophysics, **79**, no. 3, A19–A26, doi: 10.1190/geo2013-0398.1.
Berkhout, A. J., 1985, Seismic migration: Imaging of acoustic energy by wave field extrapolation (A. Theoretical aspects) (3 ed.): Elsevier.
Berkhout, A. J., 2012, Combining full wavefield migration and full waveform inversion, a glance into the future of seismic imaging: Geophysics, **77**, no. 2, S43–S50, doi: 10.1190/geo2011-0148.1.
Berkhout, A. J., and D. J. Verschuur, 1994, Multiple technology: Part 2, Migration of multiple reflections: 64th Annual International Meeting, SEG, Expanded Abstracts, 1679.
Berkhout, A. J., and D. J. Verschuur, 1997, Estimation of multiple scattering by iterative inversion, Part I: Theoretical considerations: Geophysics, **62**, 1586–1595, doi: 10.1190/1.1444261.
Berkhout, A. J., and D. J. Verschuur, 2005, Removal of internal multiples with the common-focus-point (CFP) approach: Part 1 — Explanation of the theory: Geophysics, **70**, no. 3, V45–V60, doi: 10.1190/1.1925753.
Berkhout, A. J., and D. J. Verschuur, 2006, Imaging of multiple reflections: Geophysics, **71**, no. 4, SI209–SI220, doi: 10.1190/1.2215359.
Biondi, B., and G. Shan, 2002, Prestack imaging of overturned reflections by reverse time migration: 72nd Annual International Meeting, SEG, Expanded Abstracts, 1284–1287.
Broggini, F., and R. Snieder, 2012, Connection of scattering principles: A visual and mathematical tour: European Journal of Physics, **33**, 593–613, doi: 10.1088/0143-0807/33/3/593.
Broggini, F., R. Snieder, and K. Wapenaar, 2014, Data-driven wavefield focusing and imaging with multidimensional deconvolution: Numerical ex-

amples for reflection data with internal multiples: Geophysics, **79**, no. 3, WA107–WA115, doi: 10.1190/geo2013-0307.1.
Claerbout, J. F., 1985, Imaging the earth's interior: Wiley-Blackwell.
da Costa Filho, C. A., G. A. Meles, and A. Curtis, forthcoming, Elastic internal multiple analysis and attenuation using Marchenko and interferometric methods: Geophysics, doi: 10.1190/geo2016-0162.1.
da Costa Filho, C. A., M. Ravasi, and A. Curtis, 2015, Elastic P- and S-wave autofocus imaging with primaries and internal multiples: Geophysics, **80**, no. 5, S187–S202, doi: 10.1190/geo2014-0512.1.
da Costa Filho, C. A., M. Ravasi, A. Curtis, and G. A. Meles, 2014, Elastodynamic Reen's function retrieval through single-sided Marchenko inverse scattering: Physical Review E, **90**, 063201, doi: 10.1103/PhysRevE.90.063201.
Fleury, C., 2013, Increasing illumination and sensitivity of reverse-time migration with internal multiples: Geophysical Prospecting, **61**, 891–906, doi: 10.1111/1365-2478.12041.
Fokkema, J., R. Van Borselen, and P. Van den Berg, 1994, Removal of inhomogeneous internal multiples: 56th Annual International Conference and Exhibition, EAGE, Extended Abstracts, doi: 10.3997/2214-4609.201409897.
Fomel, S., 1997, A variational formulation of the fast marching Eikonal solver: SEP-95: Stanford Exploration Project, 127–147.
Guitton, A., 2002, Shot-profile migration of multiple reflections: 72nd Annual International Meeting, SEG, Expanded Abstracts, 2478.
Guitton, A., B. Kaelin, and B. Biondi, 2007, Least-squares attenuation of reverse-timemigration artifacts: Geophysics, **72**, no. 1, S19–S23, doi: 10.1190/1.2399367.
Halliday, D., and A. Curtis, 2010, An interferometric theory of source-receiver scattering and imaging: Geophysics, **75**, no. 6, SA95–SA103, doi: 10.1190/1.3486453.
Jakubowicz, H., 1998, Wave equation prediction and removal of interbed multiples: 68th Annual International Meeting, SEG, Expanded Abstracts, 1527–1530.
Malcolm, A. E., B. Ursin, and M. V. de Hoop, 2009, Seismic imaging and illumination with internal multiples: Geophysical Journal International, **176**, 847–864, doi: 10.1111/j.1365-246X.2008.03992.x.
Meles, G. A., K. Löer, M. Ravasi, A. Curtis, and C. A. da Costa Filho, 2015, Internal multiple prediction and removal using Marchenko autofocusing and seismic interferometry: Geophysics, **80**, no. 1, A7–A11, doi: 10.1190/geo2014-0408.1.
Muijs, R., J. O. A. Robertsson, and K. Holliger, 2007, Prestack depth migration of primary and surface-related multiple reflections: Part I — Imaging: Geophysics, **72**, no. 2, S59, doi: 10.1190/1.2422796.
Ravasi, M., and A. Curtis, 2013, Nonlinear scattering based imaging in elastic media: Theory, theorems, and imaging conditions: Geophysics, **78**, no. 3, S137–S155, doi: 10.1190/geo2012-0286.1.
Ravasi, M., I. Vasconcelos, A. Kritski, A. Curtis, C. A. da Costa Filho, and G. A. Meles, 2015, Marchenko imaging of Volve field, North Sea: 77th Annual International Conference and Exhibition, EAGE, Extended Abstracts, doi: 10.3997/2214-4609.201412938.
Ravasi, M., I. Vasconcelos, A. Kritski, A. Curtis, C. A. da Costa Filho, and G. A. Meles, 2016, Target-oriented Marchenko imaging of a North Sea field: Geophysical Journal International, **205**, 99–104, doi: 10.1093/gji/ggv528.
Regone, C. J., 2007, Using 3D finite-difference modeling to design wide-azimuth surveys for improved subsalt imaging: Geophysics, **72**, no. 5, SM231–SM239, doi: 10.1190/1.2668602.
Reiter, E. C., M. N. Toksöz, T. H. Keho, and G. M. Purdy, 1991, Imaging with deep-water multiples: Geophysics, **56**, 1081–1086, doi: 10.1190/1.1443119.
Richardson, A., and A. E. Malcolm, 2014, Illumination compensation using Poynting vectors, with special treatment for multiples: 84th Annual International Meeting, SEG, Expanded Abstracts, 3956–3961.
Sava, P., 2007, Stererographic imaging condition for wave-equation migration: 77th Annual International Meeting, SEG, Expanded Abstracts, 3124.
Schleicher, J., J. C. Costa, and A. Novais, 2008, A comparison of imaging conditions for wave-equation shot-profile migration: Geophysics, **73**, no. 6, S219–S227, doi: 10.1190/1.2976776.
Schneider, W., 1978, Integral formulation for migration in two and three dimensions: Geophysics, **43**, 49–76, doi: 10.1190/1.1440828.
Schuster, G. T., J. Yu, J. Sheng, and J. Rickett, 2004, Interferometric/daylight seismic imaging: Geophysical Journal International, **157**, 838–852, doi: 10.1111/j.1365-246X.2004.02251.x.
Shan, G., 2003, Source-receiver migration of multiple reflections: 73rd Annual International Meeting, SEG, Expanded Abstracts, 1008–1011.
Singh, S., R. Snieder, J. Behura, J. van der Neut, K. Wapenaar, and E. Slob, 2015, Marchenko imaging: Imaging with primaries, internal multiples, and free-surface multiples: Geophysics, **80**, no. 5, S165–S174, doi: 10.1190/geo2014-0494.1.
Stark, H., 1971, An extension of the Hilbert transform product theorem: Proceedings of the IEEE, **59**, 1359–1360, doi: 10.1109/PROC.1971.8420.
Valenciano, A., and B. Biondi, 2003, 2D deconvolution imaging condition for shot-profile migration: 73rd Annual International Meeting, SEG, Expanded Abstracts, 1059–1062.
Vasconcelos, I., R. Snieder, and B. Hornby, 2008, Imaging internal multiples from subsalt VSP data — Examples of target-oriented interferometry: Geophysics, **73**, no. 4, S157–S168, doi: 10.1190/1.2944168.
Verschuur, D. J., 2006, Seismic multiple removal techniques: Past, present and future: EAGE, Education Tour Series.
Wang, B., M. Guo, C. Mason, J. Cai, S. Gajawada, and D. Epili, 2009, Wave-equation based residual multiple prediction and elimination in migration depth domain as an aid to seismic interpretation: 79th Annual International Meeting, SEG, Expanded Abstracts, 3123–3127.
Wapenaar, K., 2014, Single-sided Marchenko focusing of compressional and shear waves: Physical Review E, **90**, 063202, doi: 10.1103/PhysRevE.90.063202.
Wapenaar, K., F. Broggini, E. Slob, and R. Snieder, 2013, Three-dimensional single-sided Marchenko inverse scattering, data-driven focusing, Green's function retrieval, and their mutual relations: Physical Review Letters, **110**, 0843011, doi: 10.1103/PhysRevLett.110.084301.
Wapenaar, K., J. Thorbecke, J. van der Neut, F. Broggini, E. Slob, and R. Snieder, 2014, Marchenko imaging: Geophysics, **79**, no. 3WA39–WA57, doi: 10.1190/geo2013-0302.1.
Weglein, A. B., F. A. Gasparotto, P. M. Carvalho, and R. H. Stolt, 1997, An inverse scattering series method for attenuating multiples in seismic reflection data: Geophysics, **62**, 1975–1989, doi: 10.1190/1.1444298.
Yilmaz, Ö., 2001, Seismic data analysis: SEG.
Youn, O. K., and H. Zhou, 2001, Depth imaging with multiples: Geophysics, **66**, 246–255, doi: 10.1190/1.1444901.
Zuberi, M. A. H., and T. Alkhalifah, 2014, Generalized internal multiple imaging: Geophysics, **79**, no. 5, S207–S216, doi: 10.1190/geo2013-0287.1.